A Novel Fluorescence Lifetime Imaging System that Optimizes Photon Efficiency

Ryan A. Colyer, Claudia Lee and Enrico Gratton

Department of Biomedical Engineering

University of California, Irvine

ABSTRACT

Fluorescence lifetime imaging (FLIM) is a powerful microscopy technique for providing contrast of biological and other systems by differences in molecular species or their environments. However, the cost of equipment and the complexity of data analysis have limited the application of FLIM. We present a mathematical model and physical implementation for a low cost Digital Frequency Domain FLIM (DFD-FLIM) system which can provide lifetime resolution with quality comparable to time-correlated single photon counting methods. Our implementation provides data natively in the form of phasors. Based on the mathematical model, we present an error analysis which shows the precise parameters for maximizing the quality of lifetime acquisition, as well as data to support this conclusion. The hardware and software of the proposed DFD-FLIM method simplifies the process of data acquisition for FLIM, presents a new interface for data display and interpretation, and optimizes the accuracy of lifetime determination.

INTRODUCTION

We have developed a physical implementation and statistical model of a new method for FLIM data collection and analysis. Our approach falls in the category of the "frequency domain" approach to lifetime acquisition, yet uses a detector operating in the photon counting mode. This digital frequency domain (DFD) method overcomes the problems of duty cycle, modulation of the detector gain and expensive radiofrequency synthesizers used in the classical analog frequency domain approach. In our approach we implemented all the operations performed in a frequency-domain lifetime instrument in a digital form using a single field programmable chip. Since all operations including the generation of the light modulation frequency, the generation of the cross-correlation sampling frequency and the assignment of the time of arrival of a photon to a bin are digital, there are no calibrations or adjustments to be performed. The mathematical model presented below fully accounts for all the elements of the DFD method. In addition, the mathematical model reproduces, as a limiting case, the principle of the time-correlated single photon counting (TCSPC) approach. Therefore, on a common statistical basis we can compare the two approaches and derive some general conclusions about the relative precision of the two methods. We found that with proper system design the two methods can be made to have comparable precision. More importantly, the mathematical model was used to maximize the precision of the DFD implementation and to determine which parameters are crucial to reach optimal performance. In terms of precision of the lifetime measurement, we were able to fully quantify the effect of the instrument response including the jitter of the detection system.

Fluorescence lifetime is a fundamental spectroscopic quantity that allows quantitative analysis through several approaches, including the identification of molecular species based on lifetime, Förster Resonance Energy Transfer (FRET), contrast due to different ion concentrations, and measurements of chemical equilibria. For measurements done in a cuvette, in which spatial resolution is not needed, there are two major approaches for the acquisition of the fluorescence decay. One is based on TCSPC or time-sampling of the intensity decay after pulse excitation, and a second is based on the measurement of the harmonic response of the fluorescence system.

When spatial resolution is needed, such as with microscopy, different considerations come into play depending on the kind of microscope used. One major difference between the laser scanning confocal microscope and the camera based microscopes is that in the former the detector works in the serial mode, although there are some recent scanning instruments using multiple foci in conjunction with a camera to collect the image (Grant and others, 2005; van Munster and others, 2007). For FLIM instruments operating in the serial mode, a bottleneck in the rate of data acquisition is caused by the

recovery time of the TAC element that is common to the TCSPC based instruments.

During the last few years, several new instruments were introduced for FLIM operation in the confocal microscope by several manufacturers. As a consequence, FLIM has become more common and is now available in several labs. One of the reasons for the interest in FLIM is that FRET imaging by lifetime resolved methods is generally considered to have fewer problems with background and autofluorescence than intensity ratio methods. However, FLIM methods are limited to few labs due to the high cost of the instrumentation and the difficulty of performing lifetime analysis in many pixels simultaneously (Pelet and others, 2004). The analog frequency-domain approach offers some simplification in the analysis methods and in the laser sources used (Clegg and others, 1992). However, the traditional frequency-domain electronics operating in the radio frequency range require gain modulated detectors, radio frequency amplifiers (Gratton and Limkeman, 1983), and are not a simple addition to existing laser confocal microscopes. Whatever approach is utilized, current methods are relatively expensive, require specialized electronic and modulated sources, and involve sophisticated analysis methods to extract information about the lifetime image and the processes that produce lifetime variations in different pixels of an image (Pelet and others, 2004).

In this paper we describe new data acquisition hardware that requires minimal modifications to the configuration of common commercial laser confocal microscopes. The cost of the new electronics is minimal. We also use the phasor method of data analysis that is "native" to the proposed hardware and simplifies the calculation and presentation of lifetime images. Overall, the proposed approach has the potential to make FLIM technology more widely available. Our approach uses serial detectors in the photon counting mode, and the digital heterodyning method to acquire data which is directly analyzed in the frequency domain. The principle of the digital heterodyning method was previously described (Eid, 2002). However, the original implementation by Eid et al. (2002) used a specialized acquisition card and had limitations in terms of the duty cycle and speed of data acquisition. In this paper we develop a mathematical model of DFD-FLIM (Digital Frequency Domain FLIM). Using this model we were able to choose optimal system parameters which minimize the distribution of lifetime values. Using an FPGA chip, we have implemented a version of the digital heterodyning method which has a 100% duty cycle so that no photons are lost, operates in several harmonic frequencies simultaneously, can be used in conjunction with common detectors in commercial laser scanning microscopes, only requires a modulated light source instead of a pulsed source, has uncertainty levels comparable to TCSPC methods, and has very high throughput with a very low cost. The cost of the FPGA chip and evaluation board is below $100. The mathematical model contains, as a limiting case,

the description of data acquisition using the TCSPC method of data acquisition. Using the model, we were able to compare theoretically and experimentally the proposed DFD and the TCSPC methods and to conclude that they have the same statistical accuracy. We were also able to predict the effect of instrument jitter on the precision of the DFD approach and to conclude that there is an optimal jitter level that improves the precision of the determination of very short lifetimes.

We implemented the DFD approach in several confocal microscopes, both with 1-photon and 2-photon excitation, and with home built and commercial instruments. As shown below, the hardware collects data directly under the form of "phasors" at several harmonic frequencies simultaneously. The phasor representation of the fluorescence decay allows a very simple interpretation of the FLIM image and the calculation of FRET efficiencies without the usual translation of the decay into exponential components. (The calculation of FRET efficiencies will be described in a forthcoming publication). The phasor approach to data analysis was previously proposed by us and by others (Clayton and others, 2004; Jameson and others, 1984; Redford and Clegg, 2005). It provides a simple graphical interface for FLIM data presentation and analysis without the need of fitting the fluorescence decay at each pixel. We compared data collected with the DFD and the TCSPC method on the same sample. After optimization of the design parameters, the DFD approach gave results comparable to those obtained with TCSPC.

MATERIALS AND METHODS

Introduction to digital frequency-domain methods

Frequency domain lifetime methods are characterized by the usage of a periodic modulated excitation, for which the finite lifetime of the fluorophore results in a phase delay and demodulates the emission. These characteristics of the response at any given modulation frequency are traditionally represented by τ_p and τ_m respectively. A derivation of these equations is given by (Spencer and Weber, 1969):

$$\tau_{p,h} = \frac{1}{2\pi h f_{ex}} \tan\left(\phi_{F,h}\right) \tag{1}$$

$$\tau_{m,h} = \frac{1}{2\pi h f_{ex}} \sqrt{\frac{1}{m_{F,h}^2} - 1} \tag{2}$$

Traditional analog approaches to frequency domain acquisition use modulation of the gain of a

4

PMT or of an image intensifier. For digital frequency domain lifetime acquisition, we replace the modulation of these analog signals with a digital modulation scheme inside the data collection circuitry (rather than at the detector level) by using multiple sampling windows within each excitation period, as shown in Figure 1. Because the modulation is performed digitally, the signal can be processed by an arbitrary number of sampling windows without any loss of signal, and the PMT can be operated at full gain during the entire acquisition.

To achieve sensitivity to short lifetimes and to ensure evenly distributed sampling of the fluorescence emission, we use heterodyning between the frequency of the sampling windows and the excitation frequency of the light source, as shown in Figure 1. As will be described below, this allows us to translate the fluorescence response into a cross-correlation phase histogram, as shown in Figure 2, which contains a functional form given by the convolution of the fluorescence emission with the shape of the sampling window.

Digital Frequency Domain Hardware

We created a device called the FLIMBox, in which the digital frequency domain algorithm is implemented in a system which uses a field programmable gate array (FPGA). An FPGA is a chip which can be rapidly reprogrammed with different circuit layouts by uploading firmware, and thus serves as a convenient tool for the development of scientific hardware. The specific FPGA we used
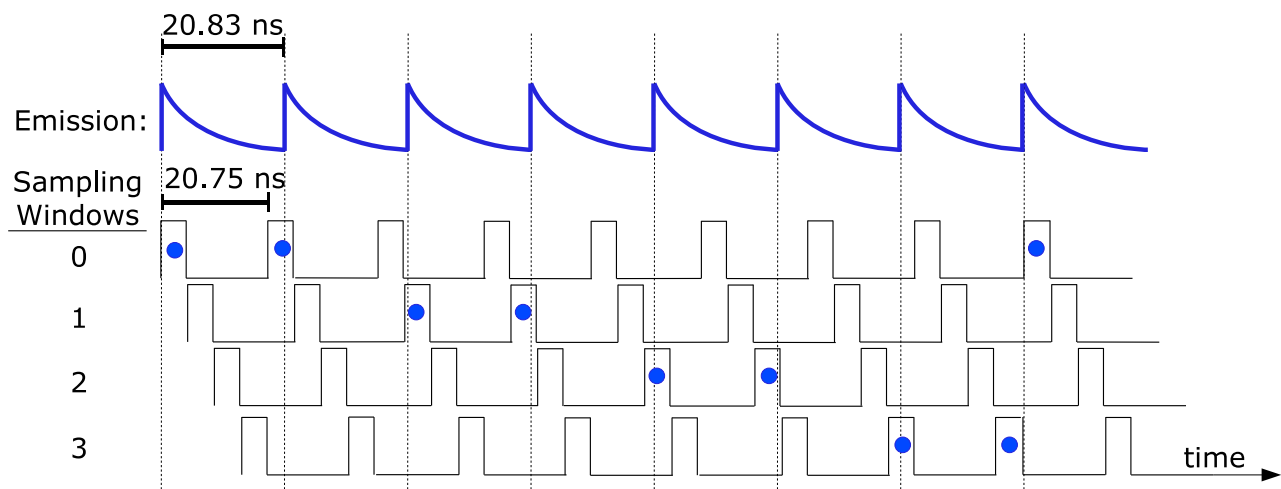

Figure 1: An illustration of the digital heterodyning principle, with exaggerated heterodyning such that $f_{cc} = f_s / 8$ instead of $f_{cc} = f_s / 256$ which we used in our implementation. Arriving photons (dots) are assigned to one of four sampling windows according to their arrival time. In the real case, the sampling windows slide through the entire period of the emission response due to the slight difference in frequencies, for a total of 256 steps.

was a Xilinx[®] Spartan[®] 3E, XC3S100E[™] (San Jose, CA), on an Avnet Electronics Marketing Evaluation Kit (Phoenix, AZ) with a Cypress EZ-USB FX2[™] chip (San Jose, CA).

The FPGA contains two digital clock managers (DCMs) which provide clock synchronization to an external clock and clock multiplication services. Each DCM multiplies an input clock frequency by n_d / m_d, where n_d and m_d are integers ranging from 1 to 32. To implement the heterodyning principle in a digital system, it is convenient to have a cross-correlation frequency which is a whole integer fraction of the sampling frequency, f_s. To reach the minimal uncertainty plateau described in the parameters optimization
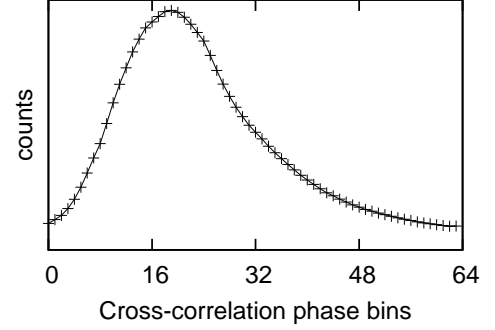

Figure 2: A histogram of counts received at each phase value of the cross-correlation period. For this figure the phase values have been divided into 64 bins. Plots such as this one contain the exponential decay of a fluorophore, convoluted by the instrument response function.

section below, at least four sampling windows are required. This can be obtained by choosing $n_1 = 32$, $m_1 = 17$, $n_2 = 32$, $m_2 = 15$, and dividing the frequency by four, such that a clock is generated which is four times the sampling clock. The resulting cross-correlation frequency of $f_{cc} = f_s / 256$, is given by:

$$f_s = \frac{n_1 n_2}{4 m_1 m_2} f_{ex} \quad \text{and} \quad f_{cc} = \left| \frac{n_1 n_2}{4 m_1 m_2} - 1 \right| f_{ex} \tag{3}$$

For example, for a 48MHz excitation frequency, a 4X clock is generated at 192.8MHz, yielding a sampling frequency of 48.188MHz and a cross-correlation frequency (the difference between the light modulation and the sampling frequency) of 188kHz. This fast 4X clock is then used as the input for a counter which tags incoming photons with the sampling window number (0 to 3) which corresponds to their arrival time.

To relate the window during which a photon arrived to a portion of the excitation period, it is necessary to know the relative phase difference between the sampling and excitation clocks. For digital stability of this phase difference measurement, this was implemented as a cross-correlation phase counter which counts at the time scale of the sampling clock, has a periodicity equal to the cross-correlation frequency, and uses negative feedback on the measurement of the excitation clock to lock on to a consistent phase relationship. This circuit enforces the same phase relationship between the cross-correlation counter and the sampling and excitation clocks each time the device is activated. Therefore the cross-correlation phase counter provides a consistent measurement of the relative phase

6

difference between the sampling and excitation clocks.

The circuit then outputs a value identifying the arrival window, $w_{arrival}$, and the cross-correlation counter value, p_{ccc}, for each photon count. For our implementation, these two values can be combined to form a cross-correlation phase index as follows:

$$p = 255 - \left[\left(p_{ccc} + \frac{256 w_{arrival}}{n_w} \right) \bmod 256 \right] \tag{4}$$

where n_w is the total number of sampling windows. This cross-correlation phase index is used to construct the cross-correlation phase histogram, $H(p)$, which is a histogram of the phase indexes for each photon detected.

A requirement for imaging in a raster-scan instrument is a mechanism for scanner synchronization, so that the system can ensure that the data for each pixel is acquired at the same physical position without significant drift. A scan enable control line was included in the chip which enables data collection only when it is active, allowing the scanner control mechanism to signal when each frame (or line) has started. We then use the total time of arrival of a photon with respect to the starting of the frame (macro-time) to divide the information into pixels, each of which has a corresponding phase histogram.

System Layout

The complete schematic layout can be seen in Figure 3, where an example is shown with the FLIMBox installed on a commercial confocal system with a modulated diode laser. We used an
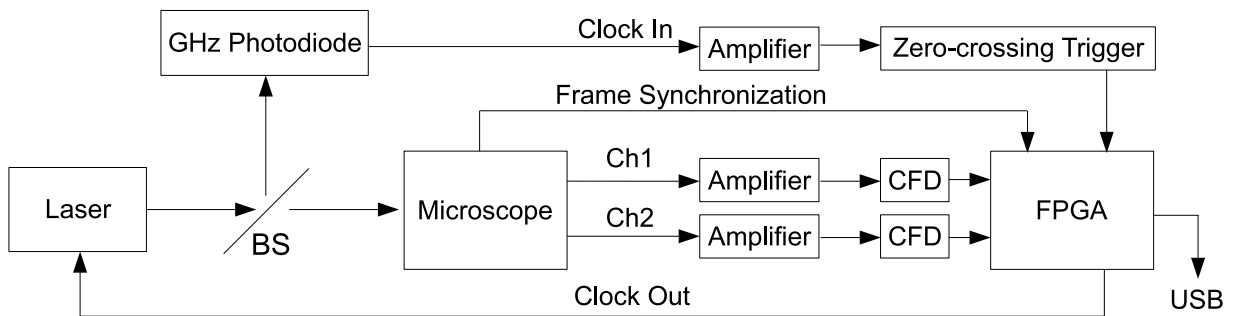

Figure 3: Experimental setup with the FLIMBox attached to a microscope. The microscope provides the signals from two detectors Ch1 and Ch2 and a Frame Synchronization signal. The FPGA unit is programmed by custom firmware to perform the digital frequency domain acquisition.

7

Olympus FluoView FV1000 (Olympus America, Center Valley, PA) with a variety of modulated diode lasers from ISS (Champaign, IL). The diode laser is driven by a 48MHz LVTTL signal produced by the FLIMBox which is high for 45° of the repetition period. In other system configurations we have also used 80MHz titanium-sapphire lasers in place of a modulated diode laser.

To provide an optical phase reference, the laser output is then split by a beam splitter which deflects a portion of the light to a GHz photodiode (Det200, Thorlabs, Newton, NJ). This photodiode signal is then amplified and sent to a zero-crossing trigger which produces a LVTTL signal that goes into the FLIMBox and serves as a frequency and phase reference for f_{ex}. The main portion of the laser is sent into the microscope. Without this optical phase reference, we found that the laser can sometimes introduce an unpredictable and significant phase shift which disrupts phase accuracy. With the optical phase reference in place, the system was stable to within 0.1° in phase.

The outputs of the photomultiplier tubes (PMTs) for two channels are sent to GHz amplifiers (ACA-4-35-N, Becker & Hickl, Berlin, Germany), which are then connected to constant fraction discriminators (CFDs) (Model 6915, Phillips Scientific, Mahwah, NJ) which trigger a LVTTL signal on the zero-slope of the PMT response when it goes past a set threshold.

The photon count LVTTL signals are processed inside of the FLIMBox on two fully independent channels. The photon arrival time information is then placed into a FIFO, from which the data is transferred via USB to a computer for processing.

The cross-correlation phase histogram at each pixel, $H(p)$, is then constructed by a computer program and used for the FLIM analysis.. The intensity image can be obtained by simply summing the points (n_p) of the phase histogram at each pixel as follows:

$$I = \sum_{p=0}^{n_p-1} H(p) \tag{5}$$

Phasor Calculation

In this work we use the phasor representation of the fluorescence decay for FLIM data analysis. The phasor approach was originally proposed by us (Jameson and others, 1984) and subsequently expanded by others (Clayton and others, 2004; Redford and Clegg, 2005). To analyze data with the phasor approach, it is necessary to calculate the intensity-normalized phasor components for harmonic h as follows:

$$g_{H,h} = \frac{1}{I} \sum_{p=0}^{n_p - 1} H(p) \cos(2\pi hp / n_p) \qquad (6)$$

$$s_{H,h} = \frac{1}{I} \sum_{p=0}^{n_p - 1} H(p) \sin(2\pi hp / n_p) \qquad (7)$$

From these two terms, the phase and modulation values are calculated according to the vector transformation equations:

$$\phi_{H,h} = \tan^{-1}\left(\frac{s_{H,h}}{g_{H,h}} \right) \qquad (8)$$

$$m_{H,h} = \sqrt{g_{H,h}^2 + s_{H,h}^2} \qquad (9)$$

The instrument response function is accounted for by scaling and rotation of the phasor using a reference phasor from a known reference lifetime. The modulation and phase values of the known lifetime are inserted into equations 24 and 25 to obtain the modulation factor and phase shift of the instrument response at each harmonic of interest. This allows one to completely account for the response of the system with a single measurement.

A global representation of FLIM images at any given harmonic frequency can be obtained by turning ϕ_F and m_F back into instrument response corrected versions of the cosine and sine values of the Fourier transform.

$$g_{F,h} = m_{F,h} \cos\left(\phi_{F,h}\right) \qquad (10)$$

$$s_{F,h} = m_{F,h} \sin\left(\phi_{F,h}\right) \qquad (11)$$

Each pair of $g_{F,h}$ and $s_{F,h}$ values can be treated as a vector called a phasor, and these values can be accumulated on a two-dimensional histogram called a phasor plot, as shown in Figure 4a.

Presenting FLIM data in this format provides a number of advantages. Since the g and s coordinates come from equations 6 and 7, they are both intensity normalized linear coordinates. The application of the instrument response only performs a scaling and a rotation, so this does not disrupt the linearity. Since g and s are linear, this means that the phasor positions of multi-exponential lifetimes are the vector sum of their single-exponential phasors. This also means that each pixel with multiple molecular species has a phasor position which is a vector sum of the phasors for each species, according to:

9

$$g_{F,h} = \sum_i f_{i,h} g_{i,h} \qquad (12)$$

$$s_{F,h} = \sum_i f_{i,h} s_{i,h} \qquad (13)$$

Where $f_{i,h}$ are the fractional fluorescence intensities of each phasor component such that:

$$\sum_i f_{i,h} = 1 \qquad (14)$$

With knowledge of the relative brightness of two species, this property of the phasors allows one to extract relative concentrations with ease.

Using equations 1 and 2 we can see that all single-exponential lifetimes occur when $\tau_p = \tau_m$, and thus when $m_{F,h} = \cos(\phi_{F,h})$ (Jameson and others, 1984). This corresponds to a semicircle on the phasor plot called the "universal circle" which is given by:

$$\left(g - \tfrac{1}{2}\right)^2 + s^2 = \left(\tfrac{1}{2}\right)^2 \qquad (15)$$

All multiexponential lifetimes are therefore linear combinations of single-exponential lifetimes, as given by equations 12-14, and therefore all multiexponential lifetimes have phasors which are inside the universal circle.
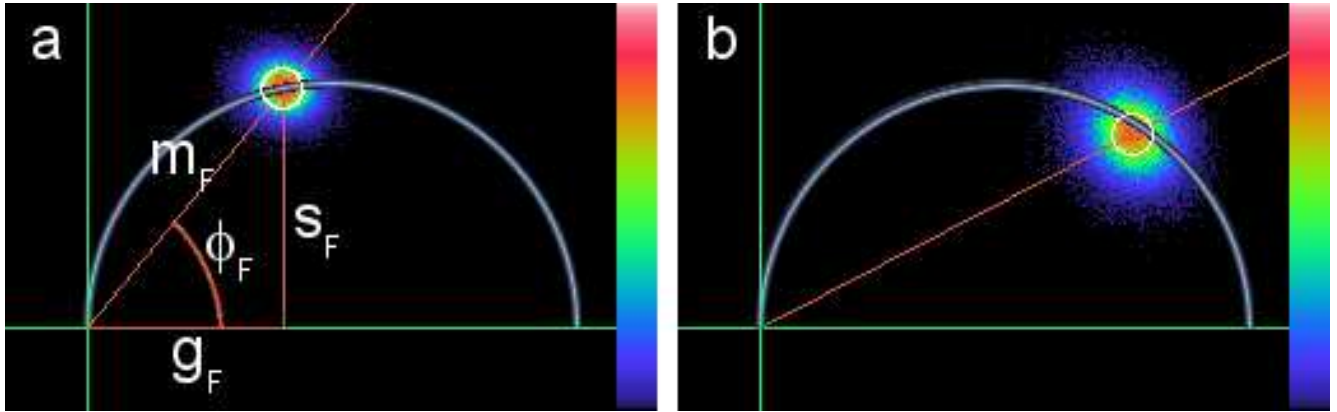

Figure 4: *The normalized phasor histograms for solutions of (a) fluorescein and (b) rhodamine B, acquired at 48MHz. Only the phasor histogram for the first harmonic is shown.*

Digital Frequency Domain FLIM Theory

To maximize the ability of DFD-FLIM hardware to determine lifetimes, we must reduce the uncertainty spread of phasors in the phasor plot. In Figure 4, where the plot is an experimental histogram of phasors at each pixel, a decrease in uncertainty would correspond to more pixels having

phasors closer to the center of the phasor distribution, or a decrease in the uncertainty of the phase and modulation. To achieve this, we developed a theoretical model of the data acquisition and processing which shows which experimental parameters are important and how to change these parameters to minimize the width of the phasor distribution.

Consider an arbitrary normalized fluorescence excitation function $E(t)$ modulated at a frequency f_{ex}, which can be written as a Fourier series,

$$E(t) = 1 + \sum_h 2m_{E,h} \cos\left(2\pi h f_{ex} t - \phi_{E,h}\right)$$

(16)

where $m_{E,h}$ is the modulation of the excitation at each harmonic, and $\phi_{E,h}$ is an arbitrary phase shift. The probability distribution for the fluorescence emission is given by the convolution between the excitation function and the fluorescence response of the fluorophores. For an arbitrary combination of fluorophores, the fluorescence response function can be written as:

$$F(t) = f_0 + \sum_i \left(\frac{f_i}{\tau_i (1 - e^{-1/(f_{ex}\tau_i)})} \right) e^{-t/\tau_i} = 1 + \sum_h 2m_{F,h} \cos\left(2\pi h f_{ex} t - \phi_{F,h}\right)$$

(17)

where τ_i are the fluorescence lifetimes, f_i are the fractional intensities, and f_0 is the contribution of the uncorrelated background. This emission is then detected by a photomultiplier tube (PMT) (or other photon counting device), a discriminator, and a logic gate, with a total time response jitter which can be approximated as a Gaussian:

$$J(t) = \frac{1}{\sigma_j \sqrt{2\pi}} e^{-t^2/(2\sigma_j^2)} = 1 + \sum_h 2m_{J,h} \cos\left(2\pi h f_{ex} t - \phi_{J,h}\right)$$

(18)

where s_j is the standard deviation of the detection time jitter, composed of a transit time spread, discriminator jitter, and triggering jitter for the digital logic. The arrival time is then resolved within the circuit into one of n_w arrival time windows, each of which is shaped as a periodic boxcar function.

$$S_{w_{arrival}}(t) = \begin{cases} f_s & \text{if} \quad \dfrac{w_{arrival}}{n_w f_s} \leq \left(t \bmod \dfrac{1}{f_s}\right) < \dfrac{w_{arrival}+1}{n_w f_s} \\ 0 & \text{otherwise} \end{cases} = 1 + \sum_h 2m_{S,h} \cos\left(2\pi h f_s t - \phi_{S,h}\right)$$

(19)

where $w_{arrival}$ is the index of the arrival time window being considered (ranging from 0 to n_w - 1), and f_s is the sampling frequency. Since this sampling process is performed digitally, every photon is counted in one of the sampling windows, resulting in a 100% duty cycle. We note that if the number of sampling windows is very large, this model corresponds to the data produced by the TCSPC method.

11

However, with TCSPC the assignment of the photon to a given bin is obtained measuring the time delay between emission and excitation by the TAC method (Time-to-Amplitude converter). In the DFD method the assignment is done by tagging the photon with a number equal to the phase shift between the sampling and excitation clocks.

We calculate the probability distribution of the detected photons by convoluting the excitation, fluorescence response, jitter of the system, and sampling window:

$$H_{w_{arrival}}(t) = E(t) * F(t) * J(t) * S_{w_{arrival}}(t) \tag{20}$$

This equation can be greatly simplified by using the convolution theorem, so that:

$$\mathcal{F}\big(H_{w_{arrival}}(t)\big) = \mathcal{F}(E(t)) \bullet \mathcal{F}(F(t)) \bullet \mathcal{F}(J(t)) \bullet \mathcal{F}\big(S_{w_{arrival}}(t)\big) \tag{21}$$

Since $E(t)$ and $S_{w,arrival}(t)$ have two different frequencies, the frequency of $H_{w,arrival}(t)$ is actually the cross-correlation frequency given by (Spencer and Weber, 1969):

$$f_{cc} = |f_s - f_{ex}| \tag{22}$$

We can see that each arrival time window represented by $S_{w,arrival}(t)$ will result in an identical

probability distribution in $H_{w,arrival}(t)$, but with a phase offset $w_{arrival} / (n_w f_{cc})$. This allows us to recombine the separate sampling windows during data processing into a single probability distribution $H(t)$. Because our analysis technique specifically utilizes the harmonics of the Fourier series, we can perform the analysis on the harmonics of $H(t)$ given by:

$$H(t) = 1 + \sum_h 2 m_{E,h} m_{F,h} m_{J,h} m_{S,h} \cos\big[2\pi h f_{cc} t - \big((\phi_{S,h} - \phi_{E,h}) + \phi_{F,h}\big)\big] \tag{23}$$

The resulting modulation of $H(t)$ for each harmonic h is given by the product of all the component modulations, as:

$$m_{H,h} = m_{E,h} m_{F,h} m_{J,h} m_{S,h} = m_{F,h} m_{IR,h} \tag{24}$$

Therefore if we know the modulation of the instrument response, $m_{IR,h} = m_{E,h} m_{J,h} m_{S,h}$, we can extract the modulation of the fluorescence lifetime response, $m_{F,h}$.

The resulting phase of $H(t)$ for each harmonic corresponds to the relative phase difference between the sampling period and the excitation period, plus the phase offset provided by the fluorescence lifetime response, as follows:

$$\phi_{H,h} = (\phi_{S,h} - \phi_{E,h}) + \phi_{F,h} = \phi_{F,h} + \phi_{IR,h} \tag{25}$$

Therefore if we know the relative phase difference between the sampling period and the excitation period, $\phi_{IR,h} = (\phi_{S,h} - \phi_{E,h})$, then we can extract the phase offset provided by the fluorescence lifetime response. Both the modulation and the phase of the instrument response can be obtained by measuring a reference sample with a known lifetime value.

Derivations similar to this section have been previously given, such as in Jameson and others. (1984). However the digital sampling windows and jitter terms were not included in previous derivations.

Optimization of the DFD Parameters

To determine the uncertainty in phasor values, we must find the standard deviation of the measured phase and modulation for each harmonic. We can perform the analysis on the phase histogram $H(p)$, which represents one period of $H(t)$, and where $0 \le p \le n_p$ - 1. To perform this error analysis, we first plot the cross-correlation phase histogram in polar coordinates for the harmonic of interest. For the first harmonic, this is a plot with $H(p)$ as the radial value, $2\pi p / n_p$ as the phase value, and where $p = n_p$ represents a complete orbit. An example is given in Figure 5.

In this coordinate system, the Fourier transform for each harmonic can be viewed graphically as the vector sum of the values plotted. $M_h = m_H N$ and ϕ_H are the magnitude and angle of this vector sum. From this graphical representation we can observe the effect of fluctuations in $H(p)$ on the values of m_H and ϕ_H. By the principles
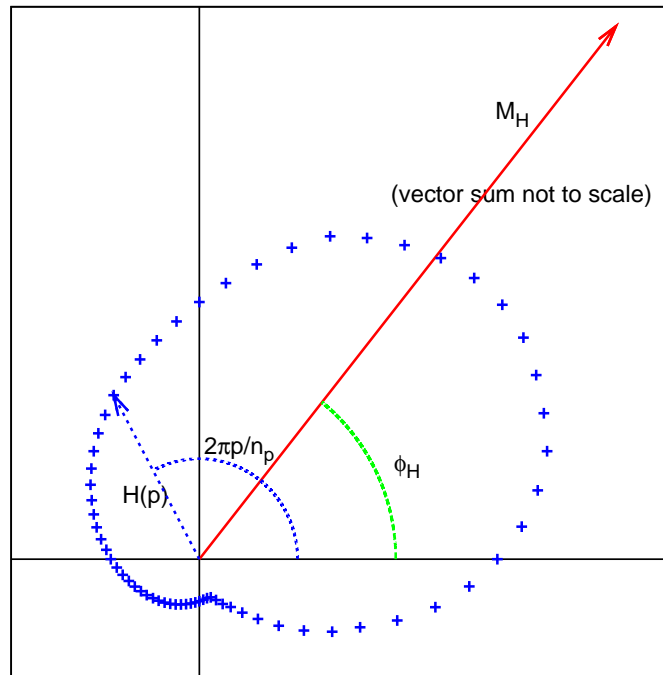

Figure 5: *The cross-correlation phase histogram bins (crosses) for fluorescein are plotted in polar coordinates, forming $n_p=64$ vectors. One vector $H(p)$ of the series is identified in the figure. The M_H vector which represents the phase and modulation of the first harmonic is produced by the vector sum of each vector in the phase histogram series.*

of vector addition, ϕ_H will only be affected by fluctuations in $H(p)$ which occur perpendicularly to the vector sum. The variances introduced by each of these components at every value of p can be added linearly. So if we consider the Poissonian error in each bin of $H(p)$ (this is the phase histogram in which every bin contains independent events), we obtain the standard deviation in phase as follows:

$$\sigma_{\phi_F,h} = \frac{1}{m_{H,h}N}\sqrt{\sum_{p=0}^{n_p-1}\left[\sqrt{H(p)}\sin(2\pi hp/n_p - \phi_{H,h})\right]^2} \tag{26}$$

$$\sigma_{\phi_F,h} = \frac{1}{m_{H,h}\sqrt{N}}\sqrt{\sum_{p=0}^{n_p-1}\left[\sqrt{1+\sum_{h'=0}^{n_p-1}2m_{H,h'}\cos(h'2\pi p/n_p - \phi_{H,h'})}\sin(2\pi hp/n_p - \phi_{H,h})\right]^2} \tag{27}$$

$$\sigma_{\phi_F,h} = \frac{\sqrt{1-m_{H,2h}\cos(2\phi_{H,h}-\phi_{H,2h})}}{m_{F,h}m_{IR,h}\sqrt{2N}} \tag{28}$$

The derivation of the expression for the standard deviation of modulation is similar, except using the fluctuations which are parallel to the vector sum, and taking into account that modulation is normalized by N, and thus fluctuations will also affect m_H via the contributions of N.

$$\delta m_{H,h} = \delta\frac{M_{H,h}}{N} = \frac{\delta M_{H,h}}{N} - \frac{M_{H,h}\delta N}{N^2} = \frac{1}{N}\sqrt{H(p)}\cos(2\pi p/n_p - \phi_{H,h}) - \frac{m_{H,h}}{N}\sqrt{H(p)} \tag{29}$$

$$\sigma_{m_F,h} = \frac{\sigma_{m_H,h}}{m_{IR,h}} = \frac{1}{m_{IR,h}N}\sqrt{\sum_{p=0}^{n_p-1}\left[\sqrt{H(p)}\left(\cos(2\pi hp/n_p - \phi_{H,h}) - m_{H,h}\right)\right]^2} \tag{30}$$

$$\sigma_{m_F,h} = \frac{\sqrt{1-2m_{H,h}^2+m_{H,2h}\cos(2\phi_{H,h}-\phi_{H,2h})}}{m_{IR,h}\sqrt{2N}} \tag{31}$$

These uncertainty values on phase and modulation can then be propagated through equations 1 and 2 to obtain the uncertainties on τ_p and τ_m:

$$\sigma_{\tau_p,h} = \frac{\sigma_{\phi_F,h}}{2\pi hf_{ex}\cos^2(\phi_{F,h})} \tag{32}$$

$$\sigma_{\tau_m,h} = \frac{\sigma_{m_F,h}}{2\pi hf_{ex}m_{F,h}^2\sqrt{1-m_{F,h}^2}} \tag{33}$$

From this analysis we can learn several insightful properties about the behavior of the phasor distribution. Firstly, the distribution of both phase and modulation decreases by the square root of the

14

number of counts in the phase histogram acquired at each pixel. Secondly, the distribution of both phase and modulation is inversely proportional to $m_{IR,h}$, the modulation of the instrument response for each harmonic. Since $m_{IR,h}$ ranges from 0 to 1, the value which produces the optimal distribution is when it is equal to 1. From consideration of $m_{IR,h} = m_{E,h}m_{J,h}m_{S,h}$ we can then immediately see that the optimal configuration places each of those component modulation values close to 1. For a square wave excitation of width θ, the modulation values as shown in Figure 6a are found by taking the Fourier transform of that square wave, which yields:

$$m_{E,h} = \frac{2}{h\theta}\sin\left(\frac{h\theta}{2}\right) \tag{34}$$

Similarly, for the sampling window, as seen in Figure 6b, the modulation values are given by:

$$m_{S,h} = \frac{n_w}{h\pi}\sin\left(\frac{h\pi}{n_w}\right) \tag{35}$$

For Gaussian system jitter, as seen in Figure 6c, the modulation values are given by:

$$m_{J,h} = e^{-2\pi^2 h^2 \sigma_j^2 f_{ex}^2} \tag{36}$$

This analysis allows us to quantitatively evaluate the design parameters required to minimize the distribution of phasors. For lifetime values obtained from the first harmonic, we can see that the modulation, and thus the information content, has reached a plateau with an excitation square wave of 90° or smaller (Figure 6a), four or more sampling windows (Figure 6b), and system jitter less than 2ns (Figure 6c). Improvements beyond this point will make only marginal improvements to the statistical uncertainties of a measurement with the first harmonic.

In our specific system configuration with a 45° square wave excitation, this produces an $m_{ex,1}$ of 0.9745, an $m_{ex,2}$ of 0.9003, and an $m_{ex,3}$ of 0.7842 at the three lowest harmonics. So even though a diode laser driven in this manner has a pulse width as wide as 2.6ns, it will still produce results of equivalent quality to a femtosecond pulsed laser for the first two harmonics.

Multiexponential Analysis

An extensive amount has been written about the extraction of component lifetimes by multi-frequency fitting (Jameson and Gratton, 1983; Gratton and others, 1984; Jameson and others, 1984; Lakowicz and others, 1984). In our imaging system used in FLIM we only excite at a single laser

repetition frequency with a pulse sufficiently narrow to contain several harmonic frequencies. Each harmonic yields 2 independent variables, the phase and modulation, so a direct relationship can be established between the number of harmonics and the number of lifetime components. For example, using 2 harmonics, two lifetime components can be calculated using an exact formula (two lifetime values, one fractional component and one background term) using the principles outlined by (Weber, 1981).

RESULTS

Solution Measurements

We evaluated the FLIMBox hardware, phasor analysis, and the above error analysis by performing solution lifetime measurements on a FLIM setup. We prepared fluorescein in a pH 10 solution, which is known to have a lifetime of 4.05ns as determined in cuvette measurements. Then we used this fluorescein solution as our lifetime reference for determining the instrument response, and also as a sample for examining the pixel uncertainty. We then prepared a solution of rhodamine B in water as an additional sample.

Figure 4a shows under the form of an image, the histogram of the phasor values for a 256x256 pixel image of fluorescein taken at 48MHz, excited with a 470nm diode laser, in the Olympus FV1000 with FLIMBox described above, with that same fluorescein sample used as the
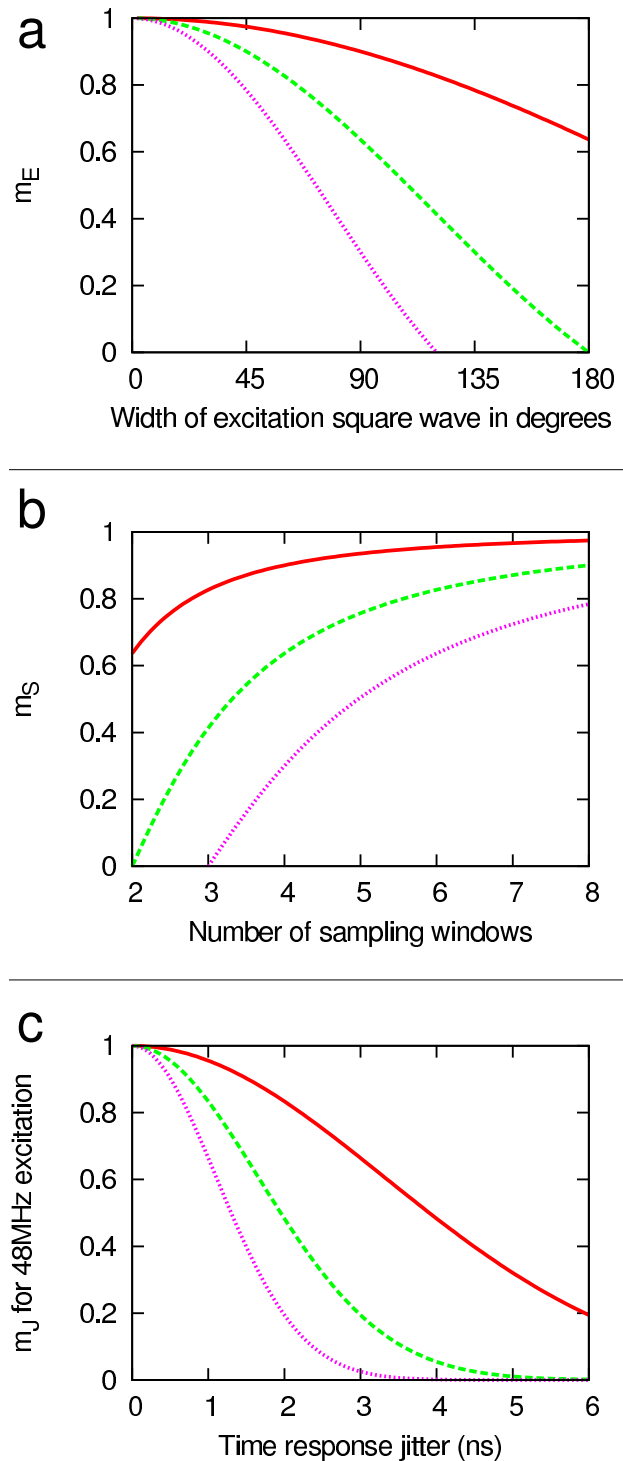

Figure 6: Plots showing the contribution to the modulation of the instrument response for the first three harmonics. (a) Square wave excitation of variable width (in degrees). (b) Number of digital sampling windows. (c) Gaussian time-response jitter of a given width (in ns). Solid, dashed, and dotted lines are for the 1st, 2nd and 3rd harmonics, respectively.

16

reference. The measurement was acquired at 200,000 counts per second, with 40 microseconds per pixel. Pixel phase histograms were accumulated until there were on the average of 538 counts in each pixel. Figure 4b shows the rhodamine B phasor plot taken on the same instrument, but with 50,000 counts per second and an average of 202 counts per pixel.

By using the error equations 28 and 31, we calculated the expected uncertainties in both phase and modulation, and we compared these to the experimental standard deviations for the fluorescein and rhodamine B measurements. We found very high correspondence between the theory and experimental results, as shown in Table 1. We repeated this comparison with many measurements under various conditions and system configurations, including for data taken with a TCSPC system, and found the equations holding in each case. This confirms that the theoretical uncertainty equations completely account for the precision of the system, and confirms that under real physical conditions, the statistical errors of a FLIM measurement can be correctly evaluated and effectively improved by the optimized parameters derived by the mathematical model of the DFD method.

TABLE 1: Phase and modulation uncertainty per pixel using the 1st harmonics at 48 MHz	Fluorescein (pH 10) *(538 counts / pixel)*		Rhodamine B (water) *(202 counts / pixel)*	
	σ_ϕ	σ_m	σ_ϕ	σ_m
Experimental	3.50°	0.035	3.86°	0.049
Theoretical	3.50°	0.035	3.83°	0.049

We also evaluated the phase and modulation lifetime values and uncertainties of the two measurements. Since the fluorescein measurement is used as a reference it is not meaningful to consider its lifetime value, since these are fixed at 4.05ns by the referencing process. However, we can still consider the uncertainties in these. The fluorescein measurement had a τ_p per pixel of 4.05 ± 0.522ns, and a τ_m per pixel of 4.05 ± 0.379ns. The predicted values for the uncertainties according to equations 32 and 33 are 0.505ns and 0.376ns. To avoid skew in the lifetime values, the mean of all lifetime values is not used to determine rhodamine B's mean lifetime. Instead, the lifetime of the center of mass of all the phasors is used, as the phasor addition is linear. For the rhodamine B measurement, the measured τ_p for each pixel was 1.723 ± 0.287ns, and the measured τ_m was 2.001 ± 0.448ns. The predicted uncertainties per pixel are 0.281ns and 0.428ns.

Note that the phasor for rhodamine B is not exactly on the universal circle, although we

expected a single exponential according to our measurement in cuvette. The phasor analysis provides an immediate and intuitive explanation for this result. In this case, the system on which the measurement was taken had background counts of 1500 per second out of a total 50,000 counts per second, which corresponds to a 3% background for the rhodamine B measurement. Since uncorrelated background counts occur at a phasor position at (0, 0) coordinate, this phasor is linearly combined according to equations 12-14 with the phasor for rhodamine B's actual lifetime. This linear combination with the uncorrelated background reduces m and therefore increases τ_m, but not the τ_p value. When the phasor contribution of the uncorrelated background is subtracted from the rhodamine B phasor, the phasor coordinate will move to the universal circle, and τ_m becomes 1.7ns.

If instead of examining the above measurements at each pixel, we use the same data to evaluate the uncertainty of the mean, rather than the uncertainty of each pixel, we find much more statistical precision. The fluorescein measurement then has a phasor point which is determined by 35 million counts, and the rhodamine measurement has a phasor point which is determined by 13 million counts. The uncertainties of the means for the fluorescein lifetimes are then 2.0ps and 1.5ps for τ_p and τ_m. Similarly for rhodamine B the uncertainties of the means are 1.1ps and 1.8ps for τ_p and τ_m. This emphasizes that the precision of lifetime measurement is not constrained by the precision of individual photon arrival times. The precision of the average value is determined by statistics, and therefore is a function of the system parameters and the number of counts. The accuracy of the phasor position determination depends on the stability of the system after it has been referenced with a known lifetime.

To evaluate the long-term stability of our system, we examined the trend of phase and modulation values over the course of hours and days using an excitation modulation of 48MHz. We determined that after an initial 45 minute warm-up period, the phase remained stable within around 0.1°, and the modulation remained stable within less than 0.001 over time periods of hours to days. These correspond to lifetime stability around 10ps for fluorescein, as given by equations 32 and 33.

For comparison with an existing standard for lifetime measurement hardware, we measured fluorescein with a 443nm diode laser modulated at 48MHz and the FLIMBox on our FV1000 setup, and with a Becker & Hickl TCSPC card (model 830, Becker & Hickl, Berlin, Germany) connected to a home-built 2-photon system using an 80MHz Titanium-Sapphire laser. According to our model, when the data are processed in the same way and for the same number of counts, the precision of the determination of the phase and modulation values should only depend on the instrument modulation factor. Since at 80 MHz, the modulation factor for fluorescein is less than at 48 MHz, we anticipated

that the precision of the data acquired with FLIMBox (at 48 MHz) should be better than the precision of data acquired with the B&H card (at 80 MHz). As can be seen in Figure 7, the phase uncertainties obtained for the measurement of fluorescein with the FLIMBox is less than that of the TCSPC system under these two sets of conditions. The relevant point here is the demonstration that both data acquisition systems reach the statistical limits in the precision of the measurement of lifetime values, and that the modulation factor and the number of photons fully account for the precision of the measurement.

Figure 7: *A comparison of the phase uncertainty for fluorescein measurements as a function of counts between a Becker & Hickl card Model 830 on an 80MHz 2-photon system (solid line, + symbol) and the FLIMBox on a diode laser system driven at 48MHz (dashed line, × symbol). Per equal counts, the uncertainty for the B&H card is higher than the FILMBox card due to the increased demodulation of the fluorescein signal at 80MHz with respect to 48MHz. However, all the uncertainties are close to the values predicted by the mathematical model when this demodulation is taken into account.*

Gerritsen et al. (2006) define a count-independent metric for the precision of a lifetime measurement as follows:

$$F = \frac{\sigma_\tau}{\tau}\sqrt{N} \tag{37}$$

By inserting equations 32 and 33 into equation 37, we are able to obtain the minimum F value (representing the highest sensitivity) for the highest modulation of the instrument response, as shown in Figure 8.

Multiexponential Analysis of ECFP

We measured the lifetime of enhanced cyan fluorescent protein (ECFP) in a 20mM Tris buffer solution with a 443 nm diode laser for excitation. Using the first and second harmonic to determine two exponential components and the amount of unmodulated background (we use an exact formula since we have two phases and two modulations and four unknown parameters), we obtained a relative contribution of 12 ± 1% for a lifetime of 0.75 ± 0.03 ns, and 88% for a lifetime of 3.17 ± 0.03 ns. The standard deviations of the lifetime determinations are obtained from 8 independent measurements of
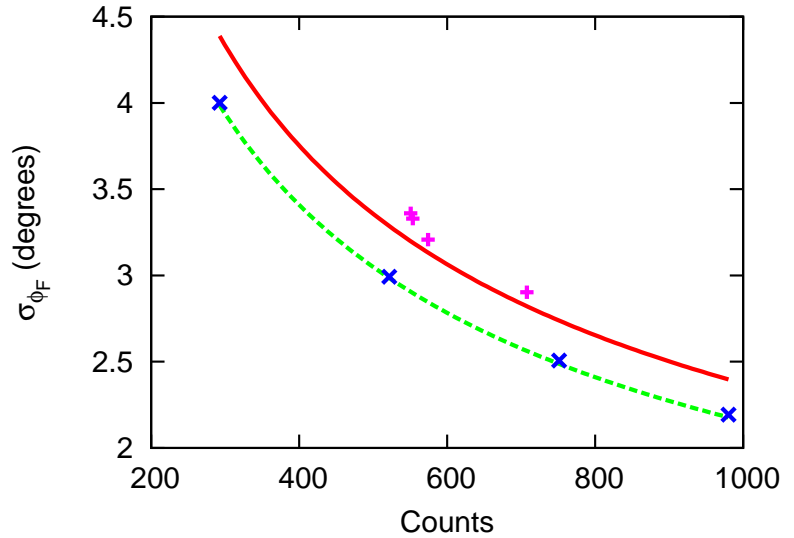
this system. We also noticed a slight spectral dependence of the relative contributions. These results correspond well with the literature, confirming the ability to extract multiple exponential components by using DFD-FLIM (Tramier and others, 2004).
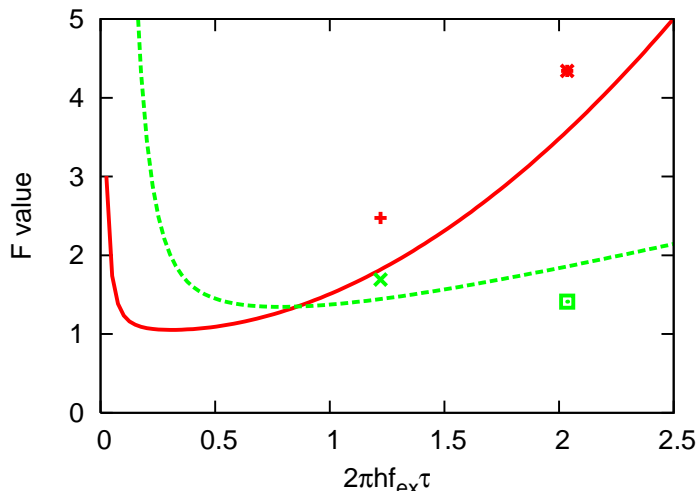

Figure 8: The theoretical minimum F values for τ_p (solid line) and τ_m (dashed line) are shown as a function of $2\pi h f_{ex}\tau$ for instrument response modulation values of 0.99. The + and × symbols show the F values for the τ_p and τ_m of fluorescein in pH 10 solution taken with the FLIMBox at 48MHz, while the ∗ and □ symbols show the F values for the same sample measured with the TCSPC system at 80MHz. The F value for τ_m of the TCSPC measurement is anomalously low due a clustering of the modulation values resulting from the dead zones at the edges of the card's phase histogram.

Fluorescence Lifetime Images

To demonstrate the ability to acquire lifetime images, and the linear combination of phasors we obtained a series of letter-shaped microchannels with a fluorescein solution in the letter "L", a rhodamine B solution in the letter "D", and a mixture of the two solutions in the letter "F". Figure 9a shows the lifetime image generated from τ_p, and Figure 9b shows the phasor plot obtained from this FLIM image. Taking advantage of the intrinsic spatial correlation in images, the phasors for this image were resampled by averaging with their nearest neighbors to improve statistical accuracy.

By using a graphical calculator inside of the Globals for Images program (LFD, Irvine, CA) which applies equations 12-14, we calculated that the "F" point on the phasor plot is 25% away from the "L" phasor, and 75% away from the "D" phasor. This shows that the phasor for the letter "F" is composed of 75% of the fluorescein solution by relative intensity.

DISCUSSION

We have developed a mathematical framework that provides an understanding of the effect of different parameters in the DFD-FLIM approach. We have shown that the experimental realization of the DFD principle in the FPGA chip gives values in very good accord with the model. This implies that the there are no additional factors (systematic or random) in the hardware implementation which are not accounted for by the mathematical model. As a consequence of the theoretical description, we
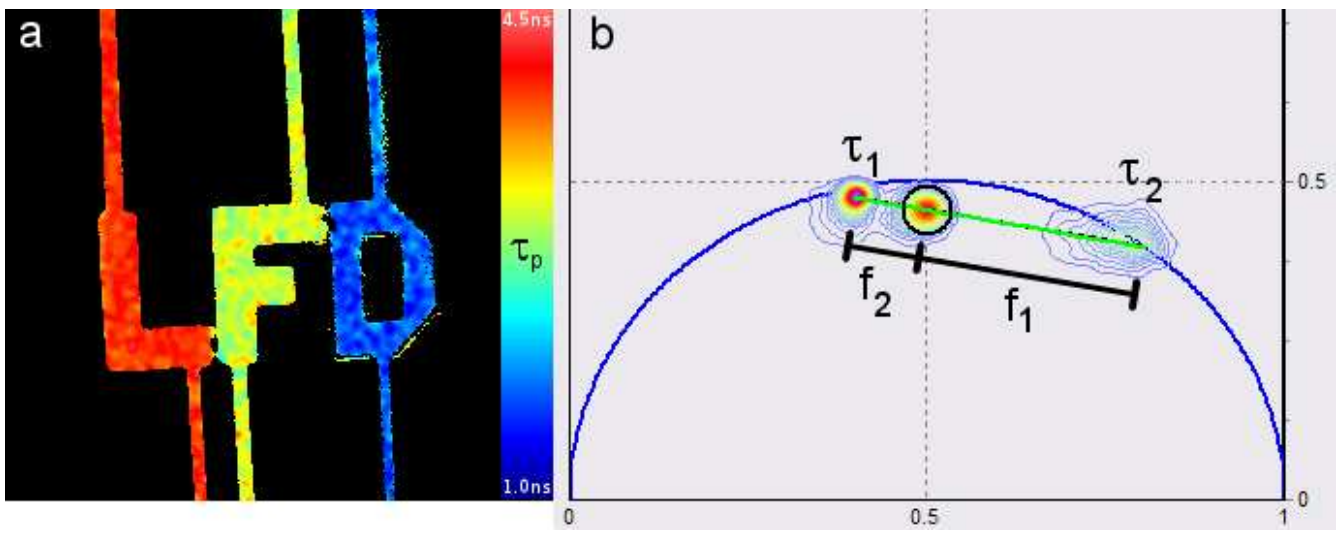
Figure 9: Microchannels with fluorescein in pH 10 solution (letter L), rhodamine B (letter D), and a combination of the two (letter F). Shown are (a) the τ_p image and (b) a phasor plot demonstrating that the phasors in the letter F are a linear combination of the phasors for the letters L and D.

have determined the system parameters which optimize the precision of phasor distributions and corresponding lifetime values. We have reached these optimal parameters in our implementation of the FLIMBox for a hypothetical system in which the lifetimes values range between 0.1ns and 10ns. We have also shown that using an optical reference for the excitation, the drifts of the physical implementation are very small, giving better than 10ps stability for the measurement of the lifetime of fluorescein at 48MHz.

In this work we provide a statistical framework that correctly predicts the errors in lifetime determination for any given sample and system configuration. Equations 28 and 31 show that the best precision of the position of the phasor (and of the lifetime value) is achieved when all the modulation factors are close to 1. This corresponds to the well-known principle that given a certain lifetime value, the best precision is obtained when the excitation pulse is narrow and repeats with a period which is much longer than the lifetime, the time windows (of the photon delay histogram) are in a large number and the instrument jitter is small. However, the value of this equation is that it allows us to quantitatively predict how much each of these factors will ultimately affect the precision of the lifetime determination. For example, we can predict that for a lifetime of about 3 ns (typical of a GFP) quasi optimal measurement conditions are obtained at excitation frequencies around 40-50 MHz with pulses of about 1-2 ns, using 4 time windows in the DFD implementation and with instrument jitter on the order of 1-2 ns. Improving on these conditions will only marginally decrease the error in the lifetime determination. All factors in equations 34-36 have very broad shapes (Figure 6) showing that the system performance degrades slowly when we move away from the optimal conditions. Therefore it is possible to design a system which is quasi-optimal over a relatively broad range of lifetime values. This evaluation resulted in the design of the very simple and cheap system of data acquisition for FLIM presented in this paper.

21

A striking difference between the DFD and the TCSPC approach is the small number of time windows used in the DFD (four windows) with respect to the relative large number of time bins used in the TCSPC when applied to FLIM (64 bins or more). At first sight it would appear that the small number of windows in the DFD approach will limit the capability of measuring very short lifetimes since each window ultimately is several nanoseconds wide. However, the presence of jitter and the sliding window principle makes the measurement of very short lifetime possible and the errors are comparable to the state-of-the-art TCSPC systems.

In our mathematical model of DFD, jitter was presented as a phenomenon which reduces modulation, and therefore reduces statistical accuracy. While this is true, there is also a substantial benefit of having a small amount of jitter in a system. To maintain the ability to measure very short lifetimes, it is necessary for a short lifetime response to be oversampled, so that even very small lifetime changes show up as a response in several bins of the phase histogram as shown schematically in Figure 10. This oversampling can be provided by the shape of the excitation pulse and/or by the jitter of the detection electronics. Depending on settings (laser, PMTs etc), we measured the jitter on the FV1000 system with the FLIMBox to range from 0.82ns to 2ns. This jitter, according to equations 34-36, results in modulation values ranging from 0.95 to 0.84 for the first three harmonics. The FLIMBox produces 256 bins in the phase histogram, but for memory conservation this is usually binned down to 64. This amount of jitter corresponds to an oversampling by around 3-6 bins, providing increased sensitivity to small lifetime values, with minimal expense in uncertainty. If the jitter is too large, resulting in oversampling by a large number of bins, then the precision of the measurement will reduce according to the modulation value (Equation 36) for that jitter. The effect of jitter in the determination of very short lifetime values is more complex than it will appear solely from equation 36 due to the
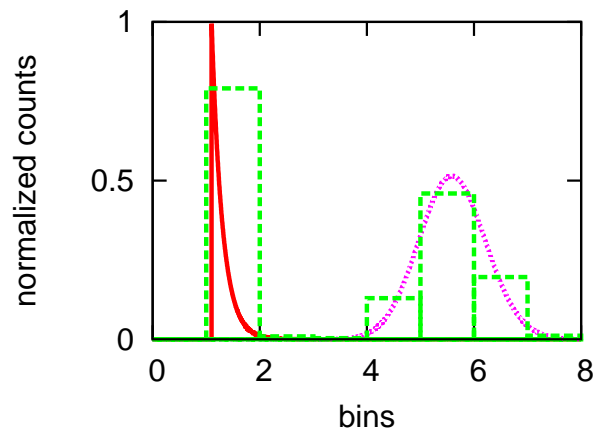

Figure 10: *With pulsed excitation, in the absence of jitter, a lifetime value much shorter than the bin size gives "delays" all in the same bin so that small changes in lifetime result in identical histograms. The solid curve at bin 1 represents this case in which the center of mass of the distribution cannot be determined with a precision better than the bin size. In the presence of jitter, the broadening of the distribution of delays gives different bin contents even if the changes in lifetime are very small. The dotted curve, which is the convolution of the solid curve with a Gaussian jitter, shows that bin 4 contains less counts than bin 6 so that the center of mass of the distribution can be determined with precision better than the bin size.*

effect of limited count statistics in any real measurements. According to Figure 10, in the absence of jitter, there is always a probability that some counts will appear in bin 2 although the majority of the counts will be in bin 1. The amount of counts in bin 2 will also depend on the precise position of the time of photon arrival inside bin 1. Therefore, if we have only a limited amount of counts, statistically we could have either no count in bin 2 or just a few counts. These discrete statistics produces a "pixelation" (in the phasor plot) of phasors corresponding to very short lifetime values. The presence of jitter reduces this "pixelation", providing a continuum of phasors centered at the correct phasor position (an equivalent effect is also present in the TCSPC approach). The important point here is that the resolution of very short lifetimes is improved and the error is reduced by the presence of a small amount of jitter and that the ultimate lifetime resolution of the DFD is only a matter of count statistics. The effect of the count statistics on the resolution of lifetimes can be precisely determined using the mathematical model and therefore a direct quantitative comparison between the DFD and TCSPC method could be done for any given implementation of the two methods.

This insight about jitter reveals new possibilities for FLIM. PMT-based systems usually have a quantum efficiency of around 25% (up to 40% for the GaAs modules), while avalanche photodiode (APD) based systems can have quantum efficiencies of over 60%. These APDs are usually avoided for lifetime measurements because they have a time response jitter on the order of a nanosecond. According to our model, the additional jitter of the APDs will have very little influence on the precision of lifetime measurements. This indicates that DFD-FLIM using APDs may actually yield an overall improvement in lifetime resolution due to the larger number of photons detected.

Our mathematical model shows that an excitation source with a pulse narrower than 90° of the repetition period is near optimal. Further reduction of the excitation pulse width only results in marginal improvement of the precision of the measurement. The DFD method, by virtue of being a frequency domain method, only works with periodic excitation. This is usually the case using pulsed lasers, however the model shows that the narrow pulses from picosecond or femtosecond lasers are not a requirement for FLIM and do not provide substantial benefit over properly modulated diode lasers in the sub-nanosecond regime.

The DFD approach increases the duty cycle of the detection to 100% as compared to the 50% duty cycle of the analog FD method. Furthermore, the 4 windows design reaches the plateau in terms of measurement precision for the first harmonic and provides a modulation of 64% for the second harmonic. There is a practical reason why we cannot increase the number of time windows to a much larger number. This is due to the maximal internal frequency of operation of the FPGA chip. For

example, to achieve 4 windows operation at about 50 MHZ, we need to generate a frequency in the chip which is factor of four larger than the modulation frequency, i.e., 200MHz. To increase the number of windows by another factor of 2 we will need to generate a frequency of 400MHz, which is above the maximum limit of the specific FPGA we have used. Other faster chips are commercially available and eventually the precision of the DFD method could be improved. However, according to Figure 6b, the improvement obtained by the 8-window design with respect to a 4-window design is marginal. Of course, if the laser repetition frequency is much lower than 50 MHz (for example 20 MHz), we could increase the number of time windows in the FPGA chip accordingly.

In a recent paper (Medine and others, 2007), it is stated that, "a principle strength of TCSPC-FLIM is statistical accuracy, and this is reflected in the ability to fit two or sometimes three exponential functions to a particular decay." We show in the section about the resolution of the decay of ECFP in two exponential components that DFD-FLIM has comparable statistical accuracy to TCSPC-FLIM for multicomponent analysis, but with substantially reduced hardware expense.

The TAC-based system we used (B&H model 830) has a 125ns dead time. The dead time limitation becomes particularly relevant in FLIM when the laser samples a very bright pixel. Saturation not only results in lost counts, but can induce significant skew on the lifetime values. Using several cards in parallel removes this limitation but at a very high cost. The FLIMBox hardware collects data at a maximum speed of one count per sampling period. The fundamental limit in count rate is due to the dead time of the discriminator (which is about 10ns) rather than the processing speed of the FPGA chip. One bottleneck of the particular FPGA we used is the size of the FIFO buffer connected to the USB interface, which limits the average (not the burst) count rate to about 2MHz.

In conclusion, DFD-FLIM provides a powerful new technique for obtaining lifetime images with a signal-to-noise and lifetime measurement ability comparable to the leading techniques in the field, yet with significantly reduced hardware expense. In addition, the theoretical model we developed reveals the system parameter values which must be chosen to optimize the efficiencies of photons for phasor analysis. When DFD-FLIM is combined with the phasor analysis methods, the resulting pair can make lifetime techniques accessible and practical for a wide variety of researchers and applications.

Acknowledgments

REFERENCES

Clayton AH, Hanley QS, Verveer PJ. 2004. Graphical representation and multicomponent analysis of single-frequency fluorescence lifetime imaging microscopy data. J Microsc 213(Pt 1):1-5.

Clegg R, Feddersen B, Gratton E, Jovin T. 1992. Time resolved imaging fluorescence microscopy. Proc. SPIE 1640, Time-Resolved Laser Spectroscopy in Biochemistry III. Lakowicz JR, editor. SPIE, Bellingham, WA, pp 448-460.

Eid J. 2002. Two-photon dual channel fluctuation correlation spectroscopy: Theory and application. PhD Thesis, UIUC.

Gerritsen HC, Draaijer A, Van den Heuvel DJ, Agronskaia AV. 2006. Fluorescence Lifetime Imaging in Scanning Microscopy. in Handbook of Biological Confocal Microscopy Third Edition. Pawley JB Editor. Springer, New York, NY:516-534.

Grant DM, Elson DS, Schimpf D, Dunsby C, Requejo-Isidro J, Auksorius E, Munro I, Neil MA, French PM, Nye E, Stamp G, Courtney P. 2005. Optically sectioned fluorescence lifetime imaging using a Nipkow disk microscope and a tunable ultrafast continuum excitation source. Opt Lett 30(24):3353-5.

Gratton E, Limkeman M. 1983. A continuously variable frequency cross-correlation phase fluorometer with picosecond resolution. Biophys J 44(3):315-24.

Gratton E, Limkeman M, Lakowicz JR, Maliwal BP, Cherek H, Laczko G. 1984. Resolution of mixtures of fluorophores using variable-frequency phase and modulation data. Biophys J 46(4):479-86.

Jameson D, Gratton E. 1983. Analysis of heterogeneous emissions by multifrequency phase and modulation fluorometry. Eastwood D, editor: American Society of Testing and Materials. 67-81 p.

Jameson DM, Gratton E, Hall R. 1984. The measurement and analysis of heterogeneous emissions by multifrequency phase and modulation fluorometry. App. Spec. Rev. 20:55-106.

Lakowicz JR, Laczko G, Cherek H, Gratton E, Limkeman M. 1984. Analysis of fluorescence decay kinetics from variable-frequency phase shift and modulation data. Biophys J 46(4):463-77.

Medine CN, McDonald A, Bergmann A, Duncan RR. 2007. Time-correlated single photon counting FLIM: some considerations for physiologists. Microsc Res Tech 70(5):420-5.

Pelet S, Previte MJ, Laiho LH, So PT. 2004. A fast global fitting algorithm for fluorescence lifetime imaging microscopy based on image segmentation. Biophys J 87(4):2807-17.

Redford GI, Clegg RM. 2005. Polar plot representation for frequency-domain analysis of fluorescence lifetimes. J Fluoresc 15(5):805-15.

Spencer RD, Weber G. 1969. Measurements of Subnanosecond Fluorescence Lifetimes with a Cross-correlation Phase Fluorometer. Annals New York Academy of Sciences 158:361-376.

Tramier M, Kemnitz K, Durieux C, Coppey-Moisan M. 2004. Picosecond time-resolved microspectrofluorometry in live cells exemplified by complex fluorescence dynamics of popular probes ethidium and cyan fluorescent protein. J Microsc 213(Pt 2):110-8.

van Munster EB, Goedhart J, Kremers GJ, Manders EM, Gadella TW, Jr. 2007.

Combination of a spinning disc confocal unit with frequency-domain fluorescence lifetime imaging microscopy. Cytometry A 71(4):207-14.

Weber G. 1981. Resolution of the fluorescence lifetimes in a heterogeneous system by phase and modulation measurements. J. Phys. Chem. 85:949-953.